

# Pressure effects on magnetic ground states in cobalt doped multiferroic $\text{Mn}_{1-x}\text{Co}_x\text{WO}_4$

Jinchen Wang,<sup>1,2,3</sup> Feng Ye,<sup>3,2,\*</sup> Songxue Chi,<sup>3</sup> Jaime A. Fernandez-Baca,<sup>3,4</sup> Huibo Cao,<sup>3</sup>  
Wei Tian,<sup>3</sup> M. Gooch,<sup>5</sup> N. Poudel,<sup>5</sup> Yaqi Wang,<sup>5</sup> Bernd Lorenz,<sup>5</sup> and C. W. Chu<sup>5,6</sup>

<sup>1</sup>*Department of Physics, Renmin University of China, Beijing 100872, China*

<sup>2</sup>*Center for Advanced Materials, Department of Physics and Astronomy,  
University of Kentucky, Lexington, Kentucky 40506, USA*

<sup>3</sup>*Quantum Condensed Matter Division, Oak Ridge National Laboratory, Oak Ridge, Tennessee 37831, USA*

<sup>4</sup>*Department of Physics and Astronomy, University of Tennessee, Knoxville, Tennessee 37996, USA*

<sup>5</sup>*Department of Physics and TCSUH, University of Houston, Houston, Texas 77204, USA*

<sup>6</sup>*Lawrence Berkeley National Laboratory, 1 Cyclotron Road, Berkeley, CA 94720, USA*

(Dated: November 12, 2018)

Using ambient pressure x-ray and high pressure neutron diffraction, we studied the pressure effect on structural and magnetic properties of multiferroic  $\text{Mn}_{1-x}\text{Co}_x\text{WO}_4$  single crystals ( $x = 0, 0.05, 0.135$  and  $0.17$ ), and compared it with the effects of doping. Both Co doping and pressure stretch the Mn-Mn chain along the  $c$  direction. At high doping level ( $x = 0.135$  and  $0.17$ ), pressure and Co doping drive the system in a similar way and induce a spin-flop transition for the  $x = 0.135$  compound. In contrast, magnetic ground states at lower doping level ( $x = 0$  and  $0.05$ ) are robust against pressure but experience a pronounced change upon Co substitution. As Co introduces both chemical pressure and magnetic anisotropy into the frustrated magnetic system, our results suggest the magnetic anisotropy is the main driving force for the Co induced phase transitions at low doping level, and chemical pressure plays a more significant role at higher Co concentrations.

PACS numbers: 75.30.Kz, 75.25.-j, 61.05.F- , 75.85.+t

There has been long pursuit for materials showing coupled magnetic and electric properties, for both technological potential and fundamental scientific interest. Inspired by the magnetic control of ferroelectric polarization in  $\text{TbMnO}_3$  [1], considerable interest has focused on the “type II” multiferroic materials where the ferroelectricity has a magnetic origin [2–6]. It can be realized through spin current or inverse Dzyaloshinskii-Moriya interaction [7–9], exchange striction [10], and  $p$ - $d$  hybridization mechanism [11, 12]. Magnetic frustration is a key ingredient in these materials where the competing interactions often lead to noncollinear spin structure and delicately balanced ground states, and the corresponding electric or magnetic properties can be easily tuned by external perturbations.

The multiferroic  $\text{MnWO}_4$  is a classic example of frustrated magnets with coupled electric and magnetic properties [13–15]. It crystallizes in the monoclinic wolframite structure (space group  $P2_1/c$ ). The edge-sharing  $\text{MnO}_6$  octahedra form zigzag chains along the  $c$  axis [Fig. 1 (a)]. When cooling,  $\text{MnWO}_4$  undergoes successive magnetic transitions [16]. The incommensurate (ICM) AF3 phase orders below 13.5 K, forming a collinear sinusoidal structure with a  $T$ -dependent magnetic wavevector. An ICM AF2 phase is stabilized between  $7 \text{ K} < T < 12.6 \text{ K}$ , with the wavevector locked at  $\vec{q} = (0.214, 0.5, -0.457)$ , hosting a spiral magnetic structure that breaks the inversion symmetry [17] and a spontaneous electric polarization along the  $b$  axis. Below 7 K, the electric polarization disappears simultaneously with the AF2 phase. The commensurate AF1 phase sets in with wavevector  $\vec{q} = (0.25, 0.5, -0.5)$ , forming a collinear  $\uparrow\uparrow\downarrow\downarrow$  configuration along the chain.

Both experimental [18, 19] and theoretical [20, 21] studies have revealed sizable long-range magnetic interactions. The system is susceptible to different perturbations including magnetic field [13, 22–25] and chemical doping [26–31].

Among chemical substitutions with either magnetic or nonmagnetic ions, the Co-doped system exhibits the most complex magnetic properties [32–38]. Only a few percent of cobalt suppresses the AF1 magnetic structure and stabilizes the AF2 phase. Further doping above  $x = 0.075$  changes the spin structure into another spiral configuration (AF5 phase) accompanied by polarization flipping into the  $ac$  plane [35, 37]. When the Co concentration goes beyond  $x = 0.15$ , the polarization changes back to the  $b$  axis, and the magnetic structure forms a conical configuration with two modulation vectors of both AF2 spiral and AF4 collinear components [35, 36]. To understand the successive changes of magnetic and electric polarization states, Liang *et al.* discussed the coupling between polarization and magnetic order parameters, which is a high order term in the free energy expansion [39]. The transition is also discussed as the result of competing magnetic anisotropy field between Mn and Co ions [40, 41]. The importance of anisotropy is indeed underscored by the distinct phase diagrams for different magnetic dopants [26, 28, 30, 31]. Besides,  $\text{Co}^{2+}$  also introduces a different chemical pressure due to its smaller ionic size, which is known as an important tuning parameter in magnetically frustrated systems. Earlier pressure measurements on pure  $\text{MnWO}_4$  have revealed the evolution of the crystal structure and a phase transition to triclinic symmetry around 18–25 GPa [42–46]. But the

pressure effect on magnetic structures remains unclear. In this paper, we present the magnetic phase evolution of  $\text{Mn}_{1-x}\text{Co}_x\text{WO}_4$  under hydrostatic pressure. Pressure has a pronounced effect at high doping regime, where it induces a spin-flop transition and drives the system in a strikingly similar manner as Co doping. The similarity is also found in the crystal structure evolution, thus suggesting the chemical pressure takes effect at high Co concentrations. In the low doping regime however, pressure has limited effect on the magnetic structures. The distinct pressure responses reveal interesting contrast between different Co concentrations.

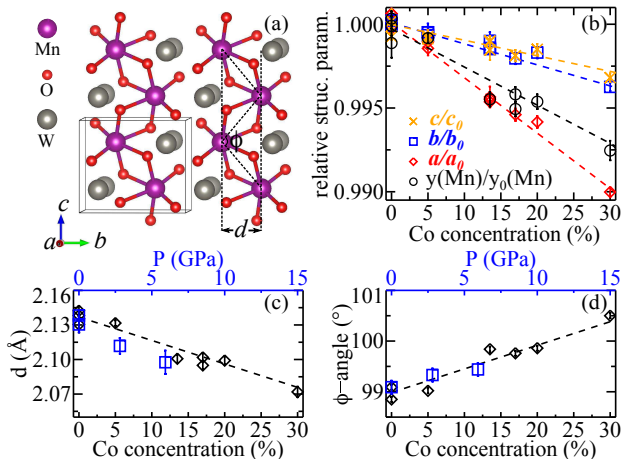


FIG. 1. (a) Crystal structure of  $\text{Mn}_{1-x}\text{Co}_x\text{WO}_4$ . The unit cell is denoted by a box in the lower left corner, and the Mn-Mn chain and its characteristic parameters are illustrated. The Co doping dependence of (b)  $a, b, c$  and  $y(\text{Mn})$ , (c) chain displacement  $d$  and (d) Mn-Mn-Mn angle  $\phi$ , are measured at room temperature and ambient pressure. Data in (b) are normalized to the undoped values to present the relative change. In (c) and (d), the pressure effects on the parent compound (blue) were calculated from Ref. [42] and compared with Co doping (black).

Single crystals of  $\text{Mn}_{1-x}\text{Co}_x\text{WO}_4$  ( $0 \leq x \leq 0.3$ ) were grown in a floating zone optical furnace. The chemical compositions were verified by energy-dispersive x-ray measurements and neutron diffraction refinement independently. Single crystal x-ray diffraction measurements were conducted at ambient pressure using a Rigaku XtaLAB PRO diffractometer equipped with a PILATUS 200K hybrid pixel array detector at the Oak Ridge National Laboratory (ORNL). Copper-beryllium cells were used to apply hydrostatic pressures up to 1.5 GPa for neutron diffraction experiments. Fluorinert was chosen as the pressure transmitting medium. The pressure inside the cell was monitored by measuring the lattice constant of a co-mounted NaCl single crystal. The nuclear and magnetic structures were investigated using the four circle diffractometer HB3A at the High Flux Isotope Reactor (HFIR), ORNL, with incident wavelength 1.5424 Å. The samples were also studied using the triple-axis spec-

trometer HB1A at HFIR with fixed  $E_i = 14.6$  meV, and the single crystal diffuse scattering spectrometer CORELLI at the Spallation Neutron Source. The sample temperature was regulated using a closed-cycle refrigerator at HB3A and HB1A, and a liquid Helium cryostat at CORELLI.

We present the room temperature and ambient pressure X-Ray diffraction results on  $\text{Mn}_{1-x}\text{Co}_x\text{WO}_4$  in Fig. 1, and compare with the pressure effect on pure  $\text{MnWO}_4$  (Ref. [42], [46]). A systematic change upon doping is evident. The lattice parameters along all crystallographic directions shrink linearly due to the smaller Co radius. Microscopically, the zigzag chain formed by  $\text{MnO}_6$  octahedron is characterized by the  $b$  axis displacement  $d$  and the Mn-Mn-Mn angle  $\phi$  [Fig. 1(a)]. With increasing the Co concentration, the Mn ion at Wyckoff position  $(0.5, y, 0.25)$  moves towards the center as the value of  $y$  decreases. Combined with the decreasing  $b$  axis lattice constant, the chain is effectively stretched along the  $c$ -axis, signified by the enlarged  $\phi$  angle and reduced displacement in  $d$ . Such structural modification due to Co doping, or chemical pressure, could profoundly influence the exchange interactions between neighboring magnetic ions and lead to new magnetic ground states as revealed by the neutron diffraction studies [35].

Applying hydrostatic pressure has a similar effect on the crystal structure; the change in the atomic position  $y$  of Mn ions upon pressure is unnoticeable, while the  $b$  axis lattice parameter decreases about twice as much comparing to the other two axes [42, 46]. This causes the interconnected  $\text{MnO}_6$  chain to distort in the same way as increasing the Co concentration [Fig. 1(c-d)]. To investigate the effect of pressure induced structural distortion on the magnetic ground state, we performed systematic, high-pressure neutron diffraction measurements on the doped  $\text{Mn}_{1-x}\text{Co}_x\text{WO}_4$  at  $x = 0, 0.05, 0.135$ , and  $0.17$ . Each has a distinct spin structure in the  $x$ - $T$  phase diagram where three spin-flop transitions occur at  $x = 0.02$ ,  $x = 0.075$ , and  $x = 0.15$ .

Figure 2 shows the  $T$ -dependence of the magnetic order parameters under pressure at four compositions. At lower doping ( $x = 0, 0.05$ ), the sequence of the magnetic transitions remains unchanged while the ordered moment is gradually reduced with increasing pressure. The transition temperatures of the AF3 phase for both compositions increase upon pressure at a rate  $\sim 0.45(9)$  K/GPa. The most prominent change happens at  $x = 0.135$ , where the pressure induces a spin-flop transition. At 1.5 GPa, commensurate AF4 peaks persist down to the lowest temperature, and the collinear AF1 at intermediate temperature and low- $T$  AF5 phase are replaced by the conical spin order normally occurring at higher Co-doping at ambient pressure [35, 36]. In the case of  $x = 0.17$ , although the magnetic structure remains the same all the way to  $P = 1.5$  GPa, the pressure is gradually enhancing the onset temperature of the AF4 phase and re-

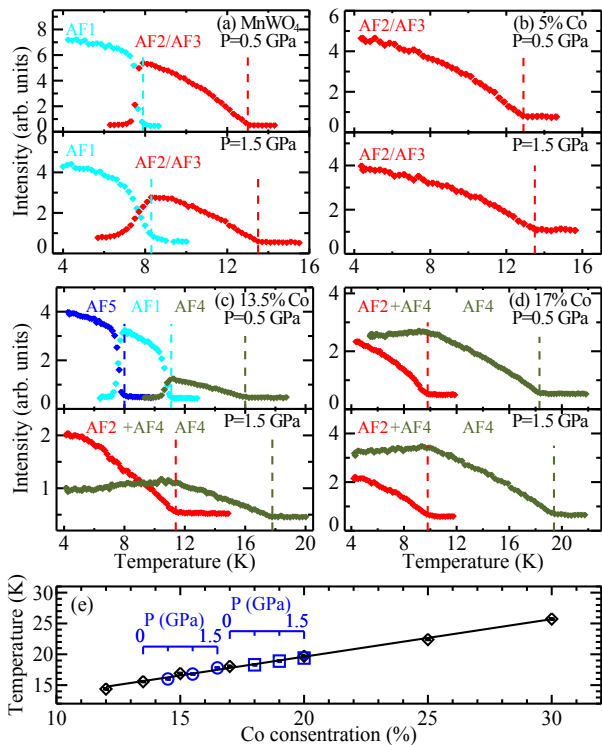


FIG. 2. Magnetic order parameters of  $\text{Mn}_x\text{Co}_{1-x}\text{WO}_4$  at (a)  $x = 0$ , (b)  $x = 0.05$ , (c)  $x = 0.135$  and (d)  $x = 0.17$  at representative pressure  $P = 0.5$  and  $1.5$  GPa. Measurements of AF5 (blue) and AF2 (red) phases were on  $(-1, 0, 1)_+$  peaks, AF1 (cyan) phase on  $(0, 1, 0)_+$  peaks and AF4 (green) phase on  $(-0.5, 1, 1)$  peaks. The onset of transition are marked by vertical dash lines. (e) Comparison of AF4 transition temperature as a function of Co-doping (black) and pressure (blue) with a scale of  $0.5$  GPa/ (Co%). The circles are the pressure results from  $x = 0.135$ , and squares are from  $x = 0.17$ .

ducing the ordered moment of the spiral AF2 component, an effect similar as increasing the cobalt concentration. All the above mentioned phases at elevated pressures were quantitative examined by magnetic structure refinements using collected Bragg peaks intensities [47]. For  $x = 0.135$  and  $0.17$ , pressure increases the transition temperature  $T_N^{\text{AF4}}$  of the collinear AF4 phase at a rate of  $\sim 1.2(1)$  K/GPa. Doping with Co alone will enhance  $T_N^{\text{AF4}}$  at a rate of  $\sim 0.61(9)$  K for every percent of Co [35, 39]. Fig. 2(e) shows the shift of  $T_N^{\text{AF4}}$  as function of doping or pressure. Applying  $0.5$  GPa hydrostatic pressure is equivalent to introducing one percent of Co. This is consistent with the structural change summarized in Figs. 1(c)-1(d).

The  $x = 0.135$  sample has the most complex pressure-induced magnetic transitions among the four compositions. Figure 3 shows the detailed measurement revealing how the magnetic configuration evolves with increasing pressure. There is a small trace of AF2 phase around 11 K at ambient pressure (Fig. 10 of Ref. [35]). It appears in a narrow temperature window of  $0.5$  K and gives way

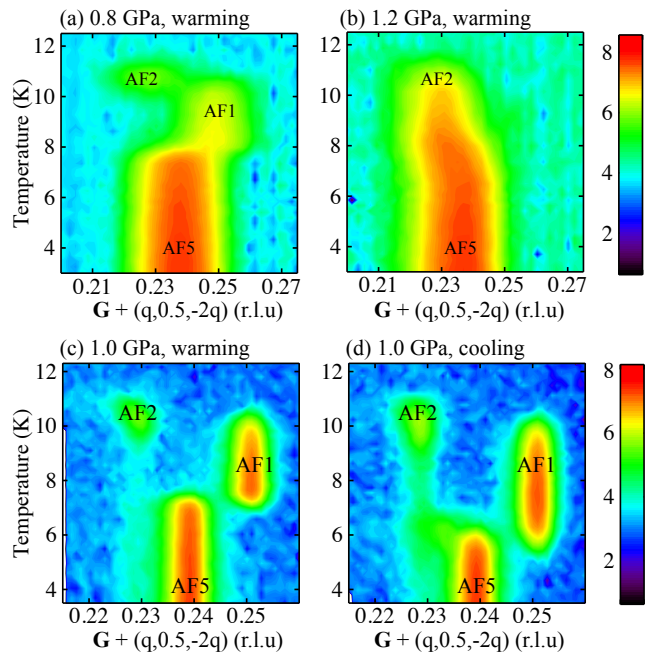


FIG. 3. The evolution of various magnetic phases of the  $x = 0.135$  sample at (a)  $0.8$  GPa, (b)  $1.2$  GPa, (c)  $1.0$  GPa in the warming process and (d)  $1.0$  GPa in the cooling process. Panels (a)-(b) and panels (c)-(d) were measured at CORELLI and HB1A, respectively. For (a) and (b) data are collected near the reciprocal lattice (rlu) vector  $\vec{G} = (-1, -1, 1)$ , which gives magnetic peaks around  $(-0.75, -0.5, 0.5)$ . Data in (c) and (d) are collected near  $\vec{G} = (0, 0, 0)$  with magnetic peaks near  $(0.25, 0.5, -0.5)$ .

to AF1 order when the system is further cooled. The AF5 order with an  $ac$ -spiral becomes the ground state at the lowest temperature. As the pressure increases, AF2 order expands in a wider temperature range as well as the AF5 phase. This shrinks the temperature window of the collinear AF1 phase as the upper(lower) boundary decreases(increases). As the pressure further increases to  $1.2$  GPa, the AF1 phase is completely suppressed and the AF2 order extends down to lower  $T$  and becomes the remaining state that competes with the AF5 phase. A strong hysteresis between cooling and warming is observed at  $1.0$  GPa [Figs. 3(c)-3(d)]. The AF2 phase tends to compete for the ground state during cooling process. The hysteresis suggests that the AF2 to AF5 transition is first order in nature, therefore clearly signifies the competition of free energy in different phases. The pressure lowers AF2's energy and eventually induces the magnetic transition at a critical point. The corresponding bulk polarization measurements [48] on the same batch of  $x = 0.135$  sample show excellent agreement with the diffraction results; at low pressure,  $P_b$  (associated with the AF2 order) initially shows an expansion of temperature window near 11 K and is then suppressed with occurrence of  $a$  axis polarization (from AF5) at low  $T$ .

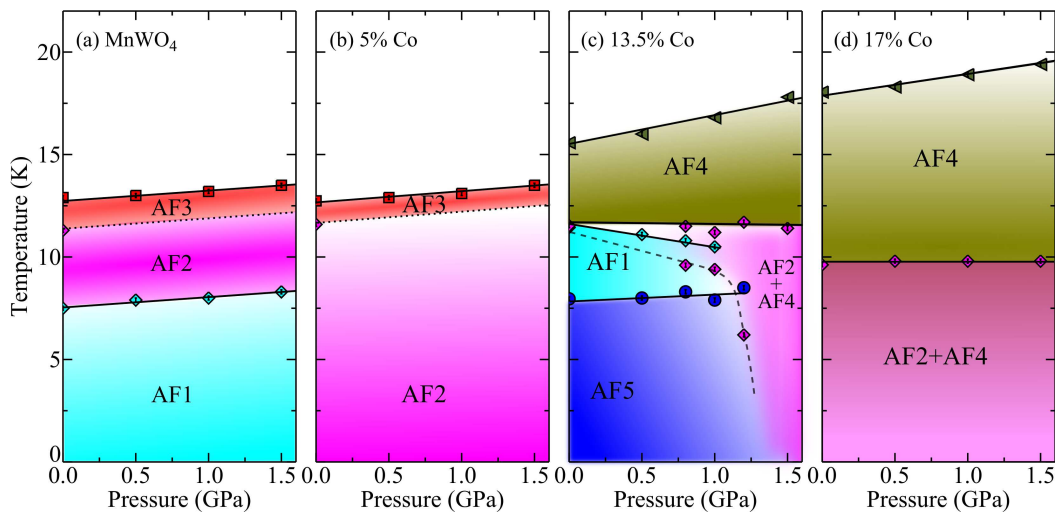


FIG. 4. The  $T$ - $P$  phase diagrams of  $\text{Mn}_{1-x}\text{Co}_x\text{WO}_4$  determined from neutron diffraction. Cyan, magenta, orange, brown, and blue represent AF1-AF5 phases, respectively. The dash line in panel (c) denotes the lower boundary of AF2 phase.

With increasing pressure, the  $b$  axis polarization gradually takes over and finally at 1.5 GPa reaches the size of the  $x = 0.17$  sample at ambient pressure.

Figure 4 illustrates the  $T$ - $P$  phase diagram at different Co compositions. Pressure has more significant effects in the high doping samples ( $x = 0.135, 0.17$ ) than the low ones ( $x = 0, 0.05$ ). At  $x = 0.135$ , the pressure-induced spin-flop transition is observed. One might speculate if the transition is due to the fragility of AF5/AF1 phases or the proximity of the  $x = 0.135$  sample to the multi-phases boundary. The AF1 phase in the undoped  $\text{MnWO}_4$  is apparently stable against pressure up to 1.5 GPa [Fig. 4 (a)], while doping a small amount of Co can quickly suppress it. The  $x = 0.135$  sample is indeed near the phase boundary where the AF5 changes to the conical phase. But it is similar for the  $x = 0.05$  sample near the boundary that separates the AF2 and AF5 states, and the undoped sample that is close to the  $x = 0.02$  boundary. If the same scale of 3% additional Co at 1.5 GPa is adopted, we expect the AF1 phase at  $x = 0$  should be completely suppressed and the  $x = 0.05$  sample is driven to the AF5 phase. However, such a pressure induced transition does not occur in these samples. It underscores distinct pressure responses between the low and high Co concentrations.

The distinct pressure responses of  $\text{Mn}_{1-x}\text{Co}_x\text{WO}_4$  reveal considerable differences in the magnetic Hamiltonian at the low and high Co concentration regime. The single-ion anisotropy of the  $\text{Co}^{2+}$  (in  $3d^7$  state) measured from the X-Ray absorption spectroscopy is much pronounced than the  $\text{Mn}^{2+}$  (in  $3d^5$  state) with half filled  $3d$  orbitals [40], and is likely to provide the largest energy change in the Hamiltonian. When Co is initially introduced, the overwhelming change in the single-ion anisotropy induces a drastic change in the magnetic ground state. This is

manifested by the quick suppression of AF1 commensurate state and the gradual rotation of AF2 spiral plane. The long-range isotropic exchange coupling term with the energy scale of 2-3 meV is highly frustrated and involves intra- and inter-chain interactions ranging from  $J_1$  to  $J_{11}$  [19]. The Dzyaloshinskii-Moriya interaction helps to stabilize the ground state in the parent compound and is important for the inversion symmetry breaking, but its overall energy scale is orders of magnitude weaker compared to other terms [49]. The competition between these interactions critically depends on the structure details such as bond distances and the Mn-O-Mn bond angle. It is desirable to investigate the detail changes of Hamiltonian upon doping and pressure in the future inelastic neutron scattering work.

The consistent scale factor of the structural change [Fig. 1(c)-(d)], the AF4 ordering temperature [Fig. 2(e)], and the pressure induced transitions at  $x = 0.135$  suggest a close correlation between the doping and pressure at high Co concentrations. Once the Co anisotropy dominates and the moment direction is locked along the Co easy axis, the magnetic structure is mainly governed by the perturbation of exchange couplings. The doping- or pressure-induced distortion in the form of chain stretching takes over and becomes the main driving force. This occurs at  $x > 0.12$  where the AF4 phase sets in. Further doping does not change the spin easy direction although Co and Mn still compete in anisotropy [50], and pressure modifies the magnetic states in a similar way as doping.

In summary, we have performed a systematic pressure study characterizing the magnetic order of multiferroic  $\text{Mn}_{1-x}\text{Co}_x\text{WO}_4$  using x-ray and neutron diffraction. We found the pressure has a significant effect on spin structure at high cobalt concentrations and induces a spin-flop transition at  $x = 0.135$ . In contrast, the magnetic

states at lower doping are rather stable against pressure. Our results reveal the balance between controlling the magnetic anisotropy and modifying the long-range magnetic interactions through structural change determines the ground state spin order, and offers a viable method to design magnetoelectric materials with desired properties.

Research at ORNL's HFIR and SNS was sponsored by the Scientific User Facilities Division, Office of Basic Energy Sciences, U.S. Department of Energy. Work at Houston is supported in part by the T.L.L. Temple Foundation, the John J. and Rebecca Moores Endowment, and the State of Texas through TCSUH, the US Air Force Office of Scientific Research, Award No. FA9550-09-1-0656. J.C. Wang acknowledges support from China Scholarship Council.

---

\* yef1@ornl.gov

- [1] T. Kimura, T. Goto, H. Shintani, K. Ishizaka, T. Arima, and Y. Tokura, *Nature* **426**, 55 (2003).
- [2] D. I. Khomskii, *J. Magn. Magn. Mater.* **306**, 1 (2006).
- [3] S. W. Cheong and M. Mostovoy, *Nature Materials* **6**, 13 (2007).
- [4] R. Ramesh and N. A. Spaldin, *Nature Materials* **6**, 21 (2007).
- [5] Y. Tokura, *J. Magn. Magn. Mater.* **310**, 1145 (2007).
- [6] Y. Tokura, S. Seki, and N. Nagaosa, *Rep. Prog. Phys.* **77**, 076501 (2014).
- [7] H. Katsura, N. Nagaosa, and A. V. Balatsky, *Physical Review Letters* **95**, 057205 (2005).
- [8] I. A. Sergienko and E. Dagotto, *Phys Rev B* **73**, 094434 (2006).
- [9] M. Mostovoy, *Physical Review Letters* **96**, 067601 (2006).
- [10] N. Hur, S. Park, P. A. Sharma, J. S. Ahn, S. Guha, and S.-W. Cheong, *Nature* **429**, 392 (2004).
- [11] C. Jia, S. Onoda, N. Nagaosa, and J. H. Han, *Phys Rev B* **74**, 224444 (2006).
- [12] C. Jia, S. Onoda, N. Nagaosa, and J. H. Han, *Phys Rev B* **76**, 144424 (2007).
- [13] K. Taniguchi, N. Abe, T. Takenobu, Y. Iwasa, and T. Arima, *Physical Review Letters* **97**, 097203 (2006).
- [14] A. H. Arkenbout, T. T. M. Palstra, T. Siegrist, and T. Kimura, *Phys Rev B* **74**, 184431 (2006).
- [15] O. Heyer, N. Hollmann, I. Klassen, S. Jodlauk, L. Bohatý, P. Becker, J. A. Mydosh, T. Lorenz, and D. Khomskii, *Journal of Physics-Condensed Matter* **18**, L471 (2006).
- [16] G. Lautenschlager, H. Weitzel, T. Vogt, R. Hock, A. Bohm, M. Bonnet, and H. Fuess, *Phys Rev B* **48**, 6087 (1993).
- [17] I. Urcelay-Olabarria, J. M. Perez-Mato, J. L. Ribeiro, J. L. García-Muñoz, E. Ressouche, V. Skumryev, and A. A. Mukhin, *Phys. Rev. B* **87**, 014419 (2013).
- [18] H. Ehrenberg, H. Weitzel, H. Fuess, and B. Hennion, *J. Phys.: Condens. Matter* **11**, 2649 (1999).
- [19] F. Ye, R. S. Fishman, J. A. Fernandez-Baca, A. A. Podlesnyak, G. Ehlers, H. A. Mook, Y. Q. Wang, B. Lorenz, and C. W. Chu, *Phys Rev B* **84**, 140401 (2011).
- [20] C. Tian, C. Lee, H. Xiang, Y. Zhang, C. Payen, S. Jobic, and M.-H. Whangbo, *Phys Rev B* **80**, 104426 (2009).
- [21] S. Matityahu, A. Aharony, and O. Entin-Wohlman, *Phys Rev B* **85**, 174408 (2012).
- [22] K. Taniguchi, N. Abe, H. Sagayama, S. Ohtani, T. Takenobu, Y. Iwasa, and T. Arima, *Phys Rev B* **77**, 064408 (2008).
- [23] H. Mitamura, T. Sakakibara, H. Nakamura, T. Kimura, and K. Kindo, *J. Phys. Soc. Jpn.* **81**, 054705 (2012).
- [24] I. Urcelay-Olabarria, E. Ressouche, A. A. Mukhin, V. Y. Ivanov, A. M. Kadomtseva, Y. F. Popov, G. P. Vorobév, A. M. Balbashov, J. L. García-Muñoz, and V. Skumryev, *Phys. Rev. B* **90**, 024408 (2014).
- [25] I. Urcelay-Olabarria, J. L. García-Muñoz, and A. A. Mukhin, *Phys. Rev. B* **91**, 104429 (2015).
- [26] F. Ye, Y. Ren, J. A. Fernandez-Baca, H. A. Mook, J. W. Lynn, R. P. Chaudhury, Y. Q. Wang, B. Lorenz, and C. W. Chu, *Phys Rev B* **78**, 193101 (2008).
- [27] L. Meddar, M. Josse, P. Deniard, C. La, G. André, F. Damay, V. Petricek, S. Jobic, M.-H. Whangbo, M. Maglione, and C. Payen, *Chem. Mater.* **21**, 5203 (2009).
- [28] R. P. Chaudhury, F. Ye, J. A. Fernandez-Baca, B. Lorenz, Y. Q. Wang, Y. Y. Sun, H. A. Mook, and C. W. Chu, *Phys Rev B* **83**, 014401 (2011).
- [29] H. W. Yu, M. F. Liu, X. Li, L. Li, L. Lin, Z. B. Yan, and J.-M. Liu, *Phys Rev B* **87**, 104404 (2013).
- [30] Y. S. Song, J. H. Chung, K. W. Shin, K. H. Kim, and I. H. Oh, *Applied Physics Letters* **104**, 4 (2014).
- [31] C. M. N. Kumar, Y. Xiao, P. Lunkenheimer, A. Loidl, and M. Ohl, *Phys Rev B* **91**, 235149 (2015).
- [32] Y.-S. Song, J.-H. Chung, J.M.S. Park, and Y.-N. Choi, *Phys Rev B* **79**, 224415 (2009).
- [33] Y.-S. Song, L. Q. Yan, B. Lee, S. H. Chun, K. H. Kim, S. B. Kim, A. Nogami, T. Katsufuji, J. Schefer, and J.-H. Chung, *Phys Rev B* **82**, 214418 (2010).
- [34] R. P. Chaudhury, F. Ye, J. A. Fernandez-Baca, Y. Q. Wang, Y. Y. Sun, B. Lorenz, H. A. Mook, and C. W. Chu, *Phys Rev B* **82**, 184422 (2010).
- [35] F. Ye, S. X. Chi, J. A. Fernandez-Baca, H. B. Cao, K. C. Liang, Y. Q. Wang, B. Lorenz, and C. W. Chu, *Phys Rev B* **86**, 094429 (2012).
- [36] I. Urcelay-Olabarria, E. Ressouche, A. A. Mukhin, V. Y. Ivanov, A. M. Balbashov, J. L. García-Muñoz, and V. Skumryev, *Phys Rev B* **85**, 224419 (2012).
- [37] I. Urcelay-Olabarria, E. Ressouche, A. A. Mukhin, V. Y. Ivanov, A. M. Balbashov, G. P. Vorobev, Y. F. Popov, A. M. Kadomtseva, J. L. García-Muñoz, and V. Skumryev, *Phys Rev B* **85**, 094436 (2012).
- [38] N. Poudel, K. C. Liang, Y. Q. Wang, Y. Y. Sun, B. Lorenz, F. Ye, J. A. Fernandez-Baca, and C. W. Chu, *Phys Rev B* **89**, 054414 (2014).
- [39] K. C. Liang, Y. Q. Wang, Y. Y. Sun, B. Lorenz, F. Ye, J. A. Fernandez-Baca, H. A. Mook, and C. W. Chu, *New J Phys* **14**, 073028 (2012).
- [40] N. Hollmann, Z. Hu, T. Willers, L. Bohatý, P. Becker, A. Tanaka, H. H. Hsieh, H.-J. Lin, C. T. Chen, and L. H. Tjeng, *Phys. Rev. B* **82**, 184429 (2010).
- [41] Y.-S. Song, J.-H. Chung, S. Hwan Chun, K. Hoon Kim, and J. Schefer, *J. Phys. Soc. Jpn.* **82**, 124716 (2013).
- [42] J. Macavei and H. Schulz, *Z. Kristall.* **207**, 193 (1993).
- [43] J. Ruiz-Fuertes, S. López-Moreno, J. López-Solano, D. Errandonea, A. Segura, R. Lacomba-Perales, A. Muñoz, S. Radescu, P. Rodríguez-Hernández,

- M. Gospodinov, L. L. Nagornaya, and C. Y. Tu, *Phys Rev B* **86**, 125202 (2012).
- [44] R. C. Dai, X. Ding, Z. P. Wang, and Z. M. Zhang, *Chemical Physics Letters* **586**, 76 (2013).
- [45] J. Ruiz-Fuertes, D. Errandonea, O. Gomis, A. Friedrich, and F. J. Manjón, *J Appl Phys* **115**, 043510 (2014).
- [46] J. Ruiz-Fuertes, A. Friedrich, O. Gomis, D. Errandonea, W. Morgenroth, J. A. Sans, and D. Santamaría-Pérez, *Phys Rev B* **91**, 104109 (2015).
- [47] See Supplemental Material.
- [48] M. Gooch, N. Poudel, B. Lorenz, K.-C. Liang, Y.-Q. Wang, Y. Y. Sun, J. Wang, F. Ye, J. A. Fernandez-Baca, and C. W. Chu, To be published.
- [49] I. V. Solovyev, *Phys. Rev. B* **87**, 144403 (2013).
- [50] J. Herrero-Martín, A. N. Dobrynin, C. Mazzoli, P. Steadman, P. Bencok, R. Fan, A. A. Mukhin, V. Skumryev, and J. L. García-Muñoz, *Phys. Rev. B* **91**, 220403 (2015).